

The Belle II Pixel Vertex Detector

A. Baur^{DESY,*} on behalf of the Belle-II DEPFET and PXD Collaboration

DESY Deutsches Elektronen-Synchrotron, 22607 Hamburg, Germany

E-mail: anselm.baur@belle2.org

The Belle II experiment at the SuperKEKB e^+e^- collider took data from 2019 to 2022 (Run 1) and is currently undergoing its planned first long shutdown (LS1). During its operational period, SuperKEKB achieved a record-breaking instantaneous luminosity of $4.7 \times 10^{34} \text{ cm}^{-2}\text{s}^{-1}$ [1] and Belle II recorded a dataset corresponding to 428 fb^{-1} . The Belle II Pixel Vertex Detector (PXD), which is the innermost sub-detector, is based on the DEpleted P-channel Field Effect Transistor (DEPFET) technology [2]. Along with the Silicon Vertex Detector (SVD) [3], utilizing double-sided silicon strips, this forms the Belle II Vertex Detector system (VXD), enabling precise reconstruction of primary and decay vertices. The PXD module features a $75 \mu\text{m}$ -thin DEPFET sensor area with varying pixel sizes from $50 \mu\text{m} \times 55 \mu\text{m}$ to $50 \mu\text{m} \times 85 \mu\text{m}$ while maintaining a hit efficiency of about 99%. Its average material budget inside the physics acceptance corresponds to $0.2\% X_0$ per layer.

PXD consist of 20 ladders arranged in two cylindrical layers around the beam axis. The Run 1 PXD was installed in a reduced configuration comprising the full inner layer (L1, eight ladders) and only two out of twelve outer layer (L2) ladders. In this article, we will illuminate the performance and operational challenges observed during its 4-year operation in a harsh environment characterized by a high beam background level.

A fully populated detector can compensate acceptance losses by redundancy and reduce the probability of wrong hit assignment introduced by higher background levels resulting from increased instantaneous luminosity. During LS1 PXD was replaced by a new, fully populated PXD2. Its commissioning and testing phase during LS1 will be described. A hit efficiency of $>98\%$ was measured in most regions using cosmic particles. The current installation schedule foresees beam operation to resume in winter 23/24.

The 32nd International Workshop on Vertex Detectors (VERTEX2023)

16-20 October 2023

Sestri Levante, Genova, Italy

*Speaker

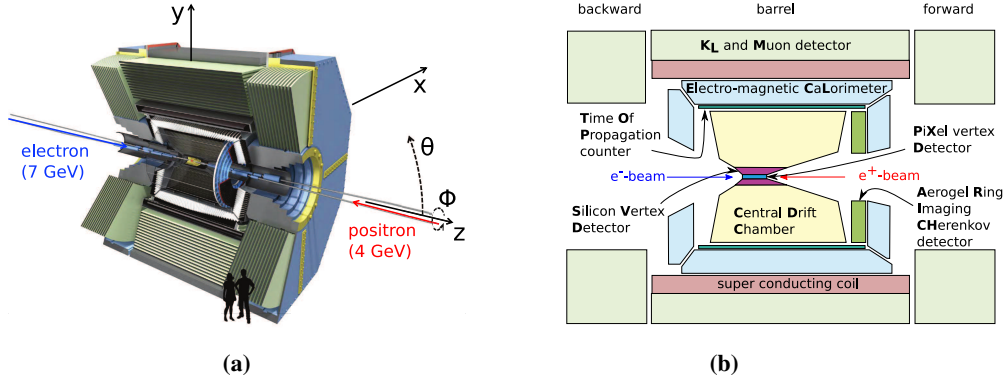


Figure 1: (a): A 3D cross section through the Belle II detector and the Belle II coordinate system [6]. (b): Cross section of the Belle II detector showing the different sub systems (adopted from [7]).

1. SuperKEKB and Belle II

The Belle II experiment is located at the SuperKEKB e^+e^- collider [4] at KEK in Tsukuba, Japan, operating at the $\Upsilon(4S)$ resonance ($10.58 \text{ GeV } c^{-2}$). With the known initial center of mass energy this enables a wide array of high precision measurements, including B, charm, tau, quarkonium physics, electroweak precision measurements and dark sector searches for new physics. The first run was performed from 2019 - 2022 (Run 1) and currently the first long shut down (LS1) takes place.

The Belle II detector and its subsystems are located around the e^+e^- interaction point, as shown in Fig. 1 [5]. The innermost subsystem is the vertex detector (VXD) composed of a pixel detector (PXD) and a silicon strip detector (SVD).

2. The Pixel Vertex Detector

The all-silicon PXD module consists of a monolithic silicon die with an integrated DEPFET sensor and metal layer connections for Surface-Mounted Devices (SMDs) and Application-Specific Integrated Circuits (ASICs) in the periphery [8]. The sensor area is thinned down to $75 \mu\text{m}$, supported by a $\sim 500 \mu\text{m}$ thick silicon (Si) frame at the module edges. This results in a low average material budget of only $\sim 0.2\% X_0$ per module within the Belle II acceptance region. Four different module types exist conditional to the position (forward, backward, inner layer, outer layer). The sensor area for inner (outer) modules measures $44.8 \times 12.5 \text{ mm}^2$ ($62.4 \times 12.5 \text{ mm}^2$). The azimuthal pixel size is always $50 \mu\text{m}$, while the longitudinal pixel size varies between $55 \mu\text{m}$ to $85 \mu\text{m}$ depending on layer and the pixel position within the active sensor area.

Pairs of forward and backward modules are glued together along the short module edges as shown in Fig. 2a forming ladder. The ladders are mounted at their ends onto the Support and Cooling Blocks (SCBs). Four inner layer ladders and six out layer ladders are mounted together on two SCBs forming a half-shell. The half-shells are mounted directly onto the beam pipe. A cross-section of the full detector is shown in Fig. 2b.

The pixel matrix is read out in a rolling shutter fashion. The switcher ASICs along the sensor edge consecutively select the pixel rows while the Drain Current Digitizers (DCDs) convert the DEPFET drain currents of the active row. The digitized values are sent to the Data Handling

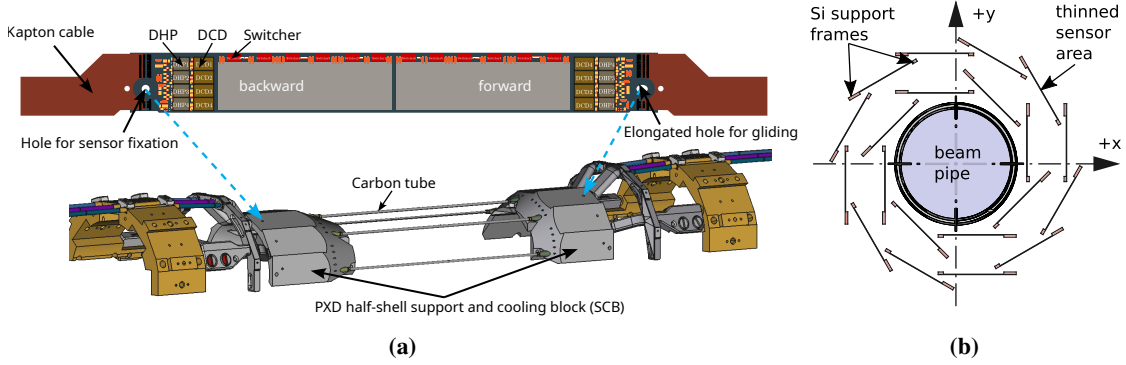


Figure 2: (a) A PXD ladder composed of two modules and the underlying support and cooling block structure where the ladders are mounted on for one half-shell. (b) Schematic of the placement of all ladders of both half-shells in wind-mill structure for full PXD (no SCBs).

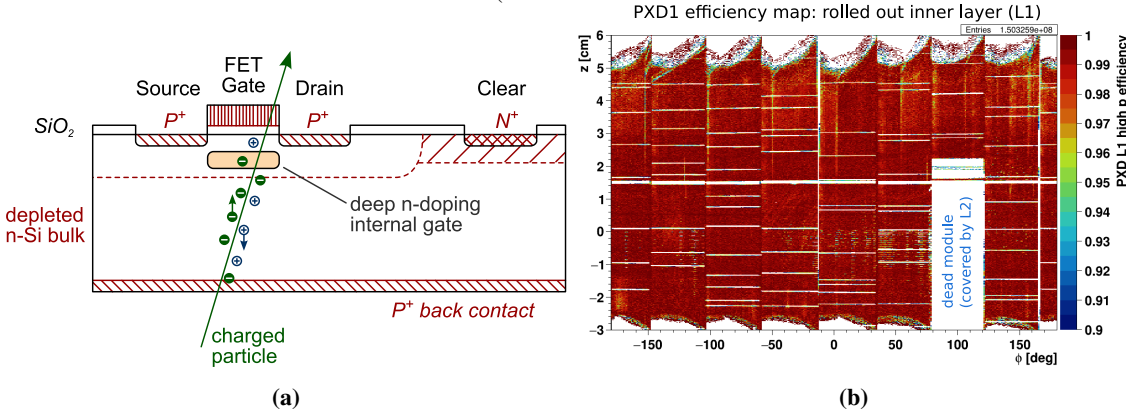


Figure 3: (a) Schematic cross section through a DEPFET pixel [9]. (b) Rolled out inner layer efficiency map as function of z and ϕ (note the 0.9 lower limit). Single ladders are visible along the z -axis and the glue gap is visible as prominent white line around $z = 1.5$ cm.

Processors (DHPs). They subtract pre-recorded pedestal values, apply an adjustable threshold and send the zero-suppressed data to the off-module readout back-end. The integral readout time of a full matrix frame is $\sim 20 \mu\text{s}$.

Each module has a power consumption of ~ 9 W which results in a total power consumption of 360 W for a fully populated system. To dissipate the heat a two-fold cooling system is installed. The majority of the heat originates from the DCD and DHP ASICs (8 W) located at the End Of Stave (EOS). It is in direct contact with the SCB, which is cooled to between -20°C to -30°C by a two-phase CO_2 system. The rest of the heat produced by the switcher ASICs and the sensor matrix (1 W) is dissipated by cooled N_2 streaming out of the end of the SCBs and from the carbon tubes connecting the SCBs (Fig. 2a lower part).

Each pixel is constructed from a Field Effect Transistor (FET) integrated on top of a fully depleted Si bulk. Under the FET channel, an internal gate is implanted as shown in Fig. 3a. When a charged particle traverses the Si bulk, electron-hole pairs are generated and separated in the electric field. The holes drift towards the back plane and the electrons towards the internal gate. The accumulated charge in the internal gate modulates the source drain current which constitutes the read out signal. After the read out, the charges are removed from the internal gate by applying a positive clear voltage to the dedicated n+ clear contact [2, 9].

3. PXD1 Operational Experiences and Challenges in Run 1

In Run 1 a partially populated version of the PXD (PXD1) was installed. It consisted of a full inner layer. To cover one malfunctioning L1 module, two already available outer layer ladders were installed covering its solid angle.

Frequent sudden beam losses were a severe problem during Run 1 after exceeding a certain bunch current. When the beam hits a collimator this can lead to high instantaneous radiation doses ($O(10\text{Gy})$ in $40\mu\text{s}$) in PXD1 which can damage the switcher ASICs. Several switcher channels (gates) or even full switchers were affected by such beam losses. In Fig. 3b 82 dead gates are visible as thin horizontal stripes as well as an unstable switcher directly next to the dead module. The damage mechanism was verified with dedicated measurements at the Mainz Microtron (MAMI) [10]. Improvements, such as faster beam loss detection and emergency power-down procedure to protect the switchers, have already been implemented. Several additional sensors were installed around the accelerator rings during LS1 to understand the origin of the sudden beam losses.

Trapped oxide charges, induced by ionizing irradiation, shift the DEPFET gate threshold over time [11]. Thus, the gate-on voltages need to be adjusted with increasing Total received Ionizing Dose (TID). Additionally, increasing bulk currents are observed in the PXD modules, which are likely caused by avalanches along guard ring structures around the sensor backside. This does not affect the efficiency of the modules, but the power supplies had to be adapted to cope with the unexpected currents. The irradiation broadens also the pedestal distributions [12]. This can be compensated by frequent calibrations.

4. PXD2

Even though the performance of the reconstructed track impact parameters is driven by the inner layer of the PXD adding the second layer yields important advantages. In Belle II, tracks are reconstructed by utilizing Central Drift Chamber (CDC) and SVD hits in a combined fit to estimate the track helix parameters. A combinatorial Kalman filter adds the PXD hits to a reconstructed track and the track helix parameters are refined in a final track fit [13]. Simulation indicates PXD hit efficiency¹ and purity² improvements to be especially significant for low transverse momentum tracks ($<0.6\text{GeV } c^{-1}$) with increasing occupancy (background). The expected gain in both cases is $\sim 20\%$ for charged particles with a transverse momentum of $0.2\text{GeV } c^{-1}$ at a background level of 2% occupancy. However, the most important feature is the physical redundancy in case regions of the inner layer sensors get damaged.

4.1 Commissioning at DESY and KEK

After initial assembly the two half-shells were individually pre-commissioned at a dedicated setup at DESY. Power supply, data read out, and CO_2/N_2 cooling systems were set up to operate ten modules ($\frac{1}{4}$ of PXD2) at a time. The commissioning setup was equipped with a movable ^{90}Sr source. Analogous to the commissioning of PXD1 in 2018, a single half-shell was mounted on an aluminum

¹Fraction of all simulated PXD hits from a particle (true hits) found in the reconstructed track.

²Fraction of true hits matched in the reconstructed track, i.e. how much background was picked up.

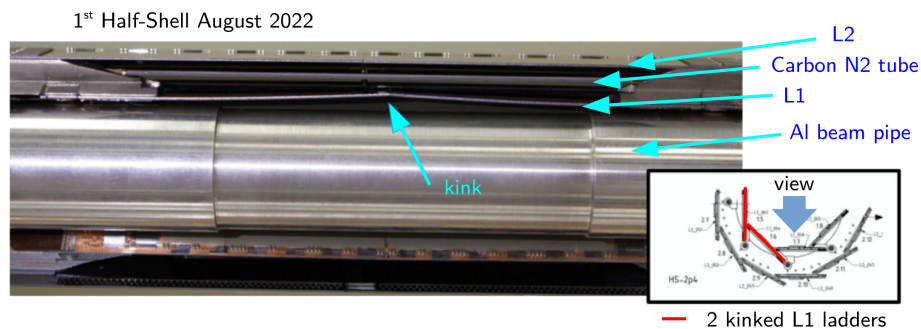


Figure 4: Broken ladders on the first PXD2 half-shell. A kink at the glue joint of one inner ladder (L1) is visible. The picture was taken from the bottom up while the half-shell was still mounted on the dummy Al beam pipe.

(Al) dummy beam pipe. Compared to before, more detailed calibration and characterization scan were planned, resulting in longer detector operation. After the first long cooled-down operation two inner ladders of the first tested half-shell had developed visible kinks (Fig. 4).

Before proceeding with the pre-commissioning, an investigation of the entire mechanical system of the PXD2 commenced, aiming to identify and address the underlying issues. Various test setups were constructed, and numerous measurements were conducted to gain a comprehensive understanding of the incident.

Several factors were identified that have contributed to the problem. One issue was the use of an Al dummy beam pipe with a large thermal expansion coefficient in the pre-commissioning setup. During long module operation when elevated air temperatures occurred in the setup, this resulted in substantial deformations of the Al dummy beam pipe. The PXD half-shell was designed to allow for small movements of the ladders and the SCB to compensate for thermal and mechanical stresses along the z-axis (along the beam pipe), but was observed to only work to a limited extent. To improve ladder gliding an additional polyethylene terephthalate (PET) foil was installed underneath the washer of the ladder mounting screw and its torque reduced without any significant loss of cooling efficiency. Additionally, the SCB was statically fixed to the beam pipe to avoid potential tilting.

The half-shell with the kinked ladders was completely disassembled and reconstructed. In total four compromised ladders were replaced. In March 2023 PXD2 was shipped to KEK for the final commissioning.

At KEK PXD2 was assembled onto a newly produced beam pipe inherently less prone to thermal deformation. In addition to environment monitoring, an alarm system, and cameras were employed to monitor the ladder bending. The commissioning at KEK started with a careful cooling operation followed by a successive and symmetric module operations until the full detector was powered. In the final beam-pipe setup with adjusted cooling parameters a significant bending of two outer layer ladders was observed (sagitta < 1 mm). Endurance tests at DESY showed that unpowered single ladders can withstand $O(10k)$ bowing cycles of up to 2 mm sagitta at room temperature without sustaining mechanical damage.

After verifying full PXD2 operability, the old VXD was extracted. Visual inspections of PXD1 showed no visible mechanical damage after 4 years of operation. The original SVD halves were installed around the PXD2 detector (Fig. 5) and the new VXD was then finally installed in the

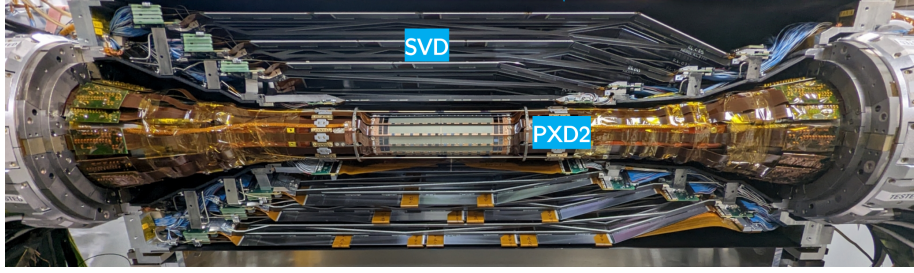


Figure 5: The new VXD. The full PXD2 and a SVD-half is visible before closing.

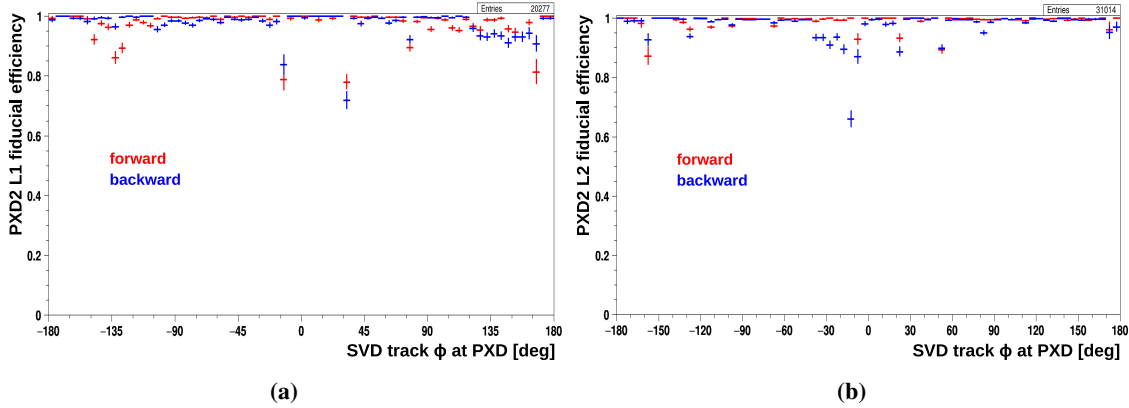


Figure 6: (a) PXD2 inner layer hit efficiency and (b) outer layer hit efficiency by first cosmic particles.

Belle II detector in August 2023.

4.2 First Cosmic Particles Measured

After the installation in the Belle II detector, first cosmic particles were recorded. A detector alignment per module was performed for the VXD. Six rigid body alignment parameters and seven deformation parameters were determined for each VXD sensor to improve the matching of the PXD2 hits with tracks reconstructed in the CDC and SVD. The spacial projection of the PXD2 hits after alignment allowed a quantification of the ladder bowing. For layer two, two ladders with a sagitta of up to ≈ 1 mm were identified. Therefore, further optimization of the cooling system is under consideration.

Reconstructed SVD tracks were used to measure a first hit efficiency of the new PXD2 (Fig. 6). Inefficient regions in Fig. 6a (e.g. at $\phi \approx 30^\circ$) are visible due to cosmic tracks not aligning with the PXD geometry. The dips at $\phi \approx -15^\circ$ and $\phi \approx 165^\circ$ originate from gaps between the two half-shells. Four modules need further tuning and optimization. Two out of these had a large number of noisy pixels masked e.g. in the inner layer around $\phi \approx 135^\circ$ (Fig. 6a) or in the outer layer around $\phi \approx -30^\circ$ (Fig. 6b). Excluding these regions, a hit efficiency of $>98\%$ was measured in most of the detector regions.

5. Summary and Outlook

After four years of successful operation, PXD1 was replaced by the new fully populated PXD2. It was installed in the Belle II detector, despite some throwbacks such as broken ladders during

long operation in the pre-commissioning setup. All 40 modules are operable but four modules need further optimization. First cosmic particle data showed in most regions a hit efficiency of $>98\%$. Two ladders exhibit significant bending, albeit to an extent that was unproblematic during endurance tests. Further optimization in the cooling system is under consideration. The operational life of PXD2 is expected to last at least until the next long shutdown within this decade.

Currently, the Belle II experiment is under commissioning, and the beam operation is expected to be resumed this winter (2023/2024).

References

- [1] D. Zhou, K. Ohmi, Y. Funakoshi and Y. Ohnishi, *Luminosity performance of superkekb*, [2306.02692](#).
- [2] J. Kemmer and G. Lutz, *New detector concepts*, *NIMA* **253** (1987) 365.
- [3] Y. Uematsu, K. Adamczyk, L. Aggarwal, H. Aihara, T. Aziz, S. Bacher et al., *The silicon vertex detector of the Belle II experiment*, *NIMA* **1033** (2022) 166688.
- [4] K. Akai, K. Furukawa and H. Koiso, *Superkekb collider*, *NIMA* **907** (2018) 188.
- [5] T. Abe, I. Adachi, K. Adamczyk, S. Ahn, H. Aihara, K. Akai et al., *Belle II technical design report*, [1011.0352v1](#).
- [6] T. Hara, T. Kuhr and Y. Ushiroda, *Belle II coordinate system and guideline of Belle II numbering scheme*, Aug, 2011.
- [7] A. Baur, *Trigger studies for $e^+e^- \rightarrow \pi^+\pi^-\gamma$ and $e^+e^- \rightarrow \mu^+\mu^-$ and implementation of a new DAQ logging and monitoring system at Belle II*, Master's thesis, Karlsruhe Institute of Technology (KIT), 2020.
- [8] F. Müller, *Characterization and optimization of the prototype DEPFET modules for the Belle II Pixel Vertex Detector*, Ph.D. thesis, Ludwig-Maximilians-Universität München, July, 2017.
- [9] R. Richter, L. Andricek, P. Fischer, K. Heinzinger, P. Lechner, G. Lutz et al., *Design and technology of DEPFET pixel sensors for linear collider applications*, *NIMA* **511** (2003) 250.
- [10] J. Schmitz, *Irradiation burst studies on Belle II PXD module components*, Master's thesis, Rheinische Friedrich-Wilhelms-Universität Bonn, Bonn, 2020.
- [11] H. Schreeck, B. Paschen, P. Wieduwilt, P. Ahlburg, L. Andricek, J. Dingfelder et al., *Effects of gamma irradiation on DEPFET pixel sensors for the Belle II experiment*, *NIMA* **959** (2020) 163522.
- [12] M. Konstantinova, *Studying the pedestal current aging and pedestal compression for the pixel vertex detector in the Belle II experiment*, Master's thesis, Universität Hamburg, 2023.
- [13] V. Bertacchi, T. Bilka, N. Braun, G. Casarosa, L. Corona, S. Cunliffe et al., *Track finding at Belle II*, *Computer Physics Communications* **259** (2021) 107610.